Development of a Medium-Strength Al-Mg-Si Alloy with Optimised Zirconium Addition

Kola Immanuel Raju[1], Viswanath Ammu[2], R. Anil Kumar[3], R. N. Chouhan[4] and Anupam Agnihotri[5]
1, 3. Scientist
2. Senior Scientist
4. Senior Principal Scientist
5. Director
Jawaharlal Nehru Aluminium Research Development & Design Centre, Nagpur, India
Corresponding author: immanuelkola@jnarddc.gov.in
https://doi.org/10.71659/icsoba2025-ch012

Abstract

Al-Mg-Si (6xxx series) aluminium alloys are widely used in extrusion due to their excellent balance of strength, toughness, and extrudability. The industry is increasingly shifting toward lightweight, medium to high-strength materials, particularly for automotive and defence applications, where aluminium extrusion alloys are favoured for their high strength-to-weight ratio and recyclability. Among aluminium alloys, the 6xxx series accounts for nearly 90 % of all extrusion products, as they offer superior extrusion speeds and surface quality compared to other extrudable alloy series. However, its strength limits its applicability, requiring improvements in mechanical properties for more demanding applications.

This study focuses on modification of a medium-strength Al-Mg-Si (AA6082 based) alloy with 0.4–0.5 wt.% zirconium (Zr) addition. The influence of Zr on grain refinement, precipitation behaviour, and mechanical property enhancement was investigated using microstructural characterization techniques such as optical microscopy, scanning electron microscopy, and phases formed using X-ray diffraction. Pilot-scale billet casting and extrusion of a 60 mm tube, followed by T6 heat treatment, demonstrated the effectiveness of Zr addition. The modified composition achieved an ultimate tensile strength (UTS) of 354 MPa and an elongation up to 16 %. This study highlights the potential of Zr addition in improving the performance of 6xxx series alloys, making them suitable for medium-strength, lightweight applications in various industries.

Keywords: Aluminium, 6xxx alloy, Extrusion, Lightweighting, Zr addition.

1. Introduction

6xxx series Aluminium alloys, comprising of Al-Mg-Si system are commercially popular in the automotive and construction industries. Owing to their favorable properties, they are now gaining traction in the defense and aerospace sectors as well [1–2]. Among the 6xxx series aluminium alloys, AA6082 is widely preferred for high-strength applications. This alloy contains magnesium and silicon, which enable precipitation hardening by forming Mg_2Si precipitates (β’ and β’’), while manganese and chromium contribute to dispersoid strengthening by forming α-Al (Mn, Cr) Si dispersoids. The final properties of the alloy are influenced by its chemical composition, casting conditions, and subsequent forming processes. Extrusion of Aluminium alloys is a high temperature forming process in which recrystallization of the microstructure is an inherent and essential part of the operation. Recrystallized microstructures tend to reduce the mechanical properties of Aluminium alloys. However, transition elements like zirconium and scandium are used as high-temperature recrystallization inhibitors by forming Al_3(Sc, Zr), aiding in grain refinement and enhancing the alloy performance.

Scandium, being a rare and expensive element, limits its widespread use. Consequently, zirconium (Zr) has been more extensively utilized, though typically restricted to a maximum of 0.3 wt.%. In this study, we explored the effects of adding over 0.4 wt.% Zr to the commercially available AA6082 alloy, aiming to investigate microstructural refinement and potential improvements in mechanical properties. In cast aluminium alloys, higher Zr additions are known to refine microstructure and improve properties. Building on this, we added over 0.4 wt.% Zr to wrought AA6082 to explore similar benefits. Jan et al. showed that 0.4–0.6 wt.% Zr in Al-Ni cast alloys promoted Al_3Zr nucleation, followed by dendritic α-Al growth [3]. Feng et al reported that the interatomic spacing values of interatomic spacing misfit and interplanar mismatch between Al_3 Zr and Al are very small, implying high grain refining efficiency of Al_3Zr in Al [4].

Birol et al. reported that the simultaneous addition of 0.13 wt.% Zr and 0.15 wt.% Cr enhances recrystallization resistance, which is attributed to the formation of Al (Cr, Mn, Fe) Si and $(Al, Si)_3Zr$ dispersoid particles [5]. Similarly, Schmid et al. observed that the addition of 0.2 wt.% Zr to the AA6082 alloy resulted in a 45 MPa increase in ultimate tensile strength (UTS), primarily due to suppressed recovery and recrystallization processes, owing to a higher dispersoid density [6].

Rakhmonov et al. [7] reported that the presence of a large volume of β″ precipitates, a smaller quantity of β′ precipitates, and fine dispersoids in the alloy containing 0.5 wt.% Mn led to a significant increase in yield strength at ambient temperature by 65–75 MPa under the T5 condition compared to the base alloy lacking dispersoids.

In the present study, Mn, Si, and Zr are incorporated to introduce additional strengthening mechanisms beyond conventional Mg_2Si precipitation hardening. The combined effect of these alloying elements and the associated strengthening mechanisms is evaluated through the tensile properties of the developed alloy. The objective is to synergize dispersoid and precipitate strengthening contributions from these additions to achieve a tensile strength exceeding 350 MPa.

2. Materials and Methods

Table 1 presents the target chemical compositions of the developed alloys from previous studies. The base alloy was designed to contain Mg and Si to facilitate the formation of θ-type precipitates, while Mn and Cr were incorporated to promote the formation of α-AlMnSi dispersoids. Additionally, Zr was added to form Al_3Zr dispersoids, contributing to enhanced thermal stability and mechanical properties.

Table 1. Chemical composition of the alloys melted.

Alloys	Zr	Si	Mn	Mg	Fe	Cr	Al (Wt.%)
Wt.%	0.45	1.1	0.91	0.91	0.18	0.25	Remaining

The alloy was prepared using an Inductotherm induction furnace equipped with a 25-kg capacity crucible. High-purity Al (99.8 %) served as the base metal, and alloying elements were introduced using master alloys such as AlMn10, AlCu30, AlZr5, AlCr10, and AlSi50. Pure magnesium (99.1 %) was added towards the end of the melting process to minimize oxidation losses. The melt temperature was maintained at 700 °C during alloying and the pouring temperature is maintained at 760 °C.

Degassing tablets were used to eliminate dissolved gases, and glass fiber filter paper was placed over the mold to trap non-metallic inclusions. Grain refinement was not employed owing to Zr-induced poisoning, which adversely affects the nucleating efficiency of standard grain refiners. The molten metal was poured into a preheated crucible at approximately 750 °C. The resulting

cast billet was cylindrical in shape, with a diameter of 149.7 mm and a length of 370 mm. Chemical composition analysis was carried out using a ThermoFisher Scientific ARL iSpark 8860 Optical Emission Spectrometer (OES). Differential Scanning Calorimetry (DSC) was performed using a Netzsch instrument at a heating rate of 10 °C/min, from room temperature up to 700 °C, under an argon atmosphere. After confirming the chemical composition of the ingots, homogenization was conducted at 550 °C for 4 hours. The as-cast billet was then preheated to 460 °C for 5 hours, while the 60 mm diameter hollow die was preheated to 480 °C for 7 hours. Extrusion was carried out using a 14 MN direct extrusion press (Maker: SMS, Germany). The container, with a diameter of 152 mm (6 inches), was preheated to 420 °C. The billet was extruded into a hollow tube of 60 mm outer diameter (OD) and 55 mm inner diameter (ID) at varying ram speeds, ranging from 0.2 to 1.0 mm/s. Artificial ageing was performed on the extrudates at a temperature of 160 °C for 12 hours. The complete schematic outlining the process from casting to ageing is presented in Figure 1.

Samples were drawn for microstructural studies which were ground using SiC papers and polished to 1-micron finish using diamond paste. Mechanical characteristics such as Yield Strength (YS) and Ultimate Tensile Strength (UTS) and % elongation were determined for the as extruded, and T6 conditions. The tensile test was conducted on an INSTRON 5582 universal testing machine with a load speed of 5 mm/min at room temperature. Tensile samples were drawn as per the ASTM E-8 Standard.

For the microstructural analysis, the specimens were etched using Keller's reagent and examined with a Leica optical microscope. SEM images were captured using a JEOL JSM IT300 scanning electron microscope, equipped with energy-dispersive X-ray (EDX) from Oxford Instrumentations.

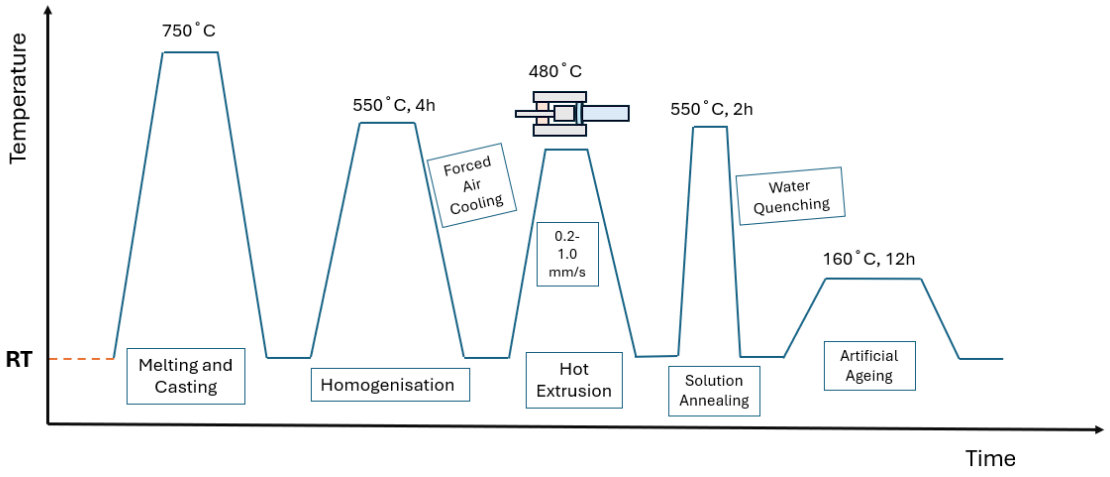

Figure 1. Schematic representation of the process employed for alloy development.

3. Results and Discussion

3.1 Phase Formations in As Cast, Homogenized and Extruded Conditions

The chemical composition of the cast billet, analyzed using spark-OES, is presented in Table 2. The target composition was successfully achieved with no significant deviations. This was accomplished through precise temperature control in the furnace and effective stirring—both automated in the induction furnace and manual—to prevent the settling of Zr at the bottom. The thermodynamic simulations were performed using Fact Sage version 8.3 with the FT Lite database shown in Figure 2. DSC analysis indicated the presence of low-melting compounds around 606 °C. However, the increase in Zr content appears to have significantly suppressed the

formation of these low-melting phases is shown in Figure 3. The simulations revealed that different stable phases form at different temperatures under equilibrium solidification conditions. The DO_{23} phase (t-Al_3Zr) was found to form at both high and low temperatures, whereas at intermediate temperatures, it was absent, and the α-Al (Fe, Mn, Cr) Si and β-AlFeSi phases became more prominent as indicated in Figure 4. These findings were corroborated by both optical microscopy and SEM imaging. The as-cast samples consisted of both α-phases and DO_{23} phases, whereas in the homogenized sample, only the α-phase was visible in the SEM images presented in Figure 5.

Table 2. Composition of the Cast Billet.

Alloy	Fe	Si	Mn	Mg	Zr	Cr	Al
Wt.%	0.14	1.12	0.97	0.94	0.42	0.23	Remaining

The DO_{23} phase is thermodynamically stable, as confirmed by EDS analysis in SEM, which identified the phase as $(Al, Si)_3Zr$ [8]. It is reported that the high silicon content in Al-Mg-Si alloys leads to the substitution of Al atoms in the lattice by Si, thereby reducing the enthalpy and favoring the formation of this phase [9]. The Mg_2Si phase is believed to precipitate at lower temperatures and has been identified as the black phase observed in the SEM microstructure. This phase contributes significantly to the precipitation hardening of the alloy. The increase in strength of the developed alloy is attributed to the coexistence of multiple strengthening mechanisms, resulting in an additional 50 MPa improvement compared to the commercially available AA6082 alloy.

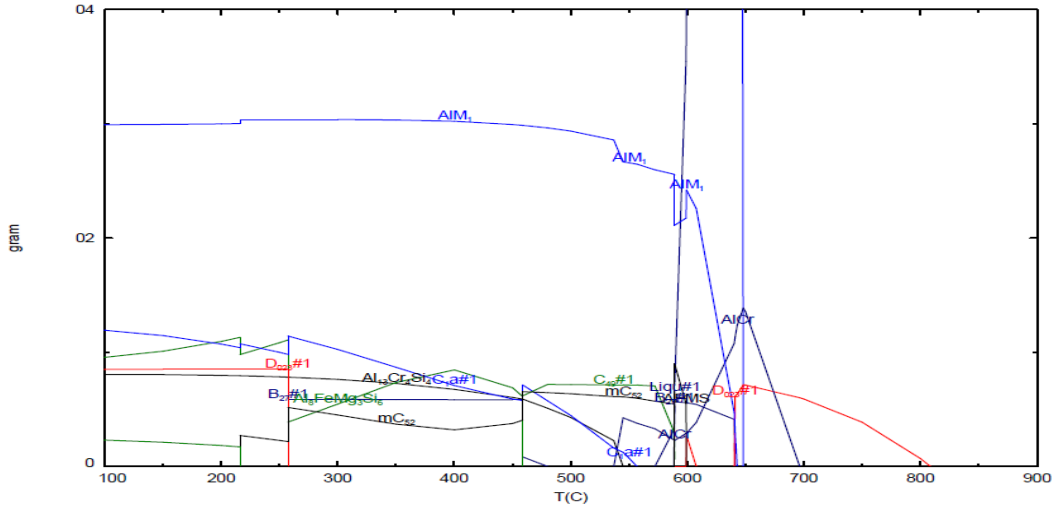

Figure 2. Equilibrium phase fractions as a function of temperature.

The cast billet was subjected to extrusion, a high-temperature process during which dynamic recrystallization (DRX) inevitably occurs, leading to the formation of coarse grains. The addition of Zr and its dispersoids aids in Zener pinning, thereby inhibiting or retarding recrystallization. Extrusion is a high-temperature deformation process during which the primary constituent particles (α-Al(Fe, Mn, Cr)Si) are fragmented, resulting in a reduction in their size. Homogenisation of the billet led to the precipitation and retention of α-Al(FeMn)Si dispersoids in the microstructure, which contributed to the retardation of dynamic recovery (DRV) and inhibition of dynamic recrystallization (DRX) during hot deformation, owing to the strong pinning effect of Mn-containing dispersoids on dislocation slip and subgrain rotation [10].

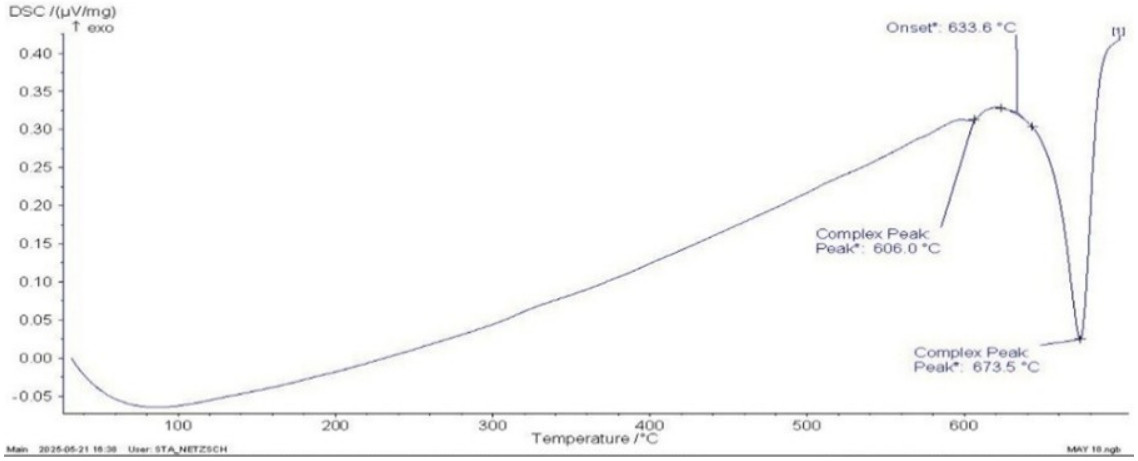

Figure 3. DSC curve of As-cast billet.

3.2 Tensile Behaviour and Fractography

Tube of 60 mm OD and 55 mm ID with ram speed varying from 0.2 mm/s to 1.0 mm/s is extruded followed by natural cooling. Tensile samples are drawn as per ASTM E-8 standard from different speeds and the samples are subjected to the Ageing process. The tensile results showed that there was an increase of strength in both Yield and Ultimate tensile strength with increasing ram speed.

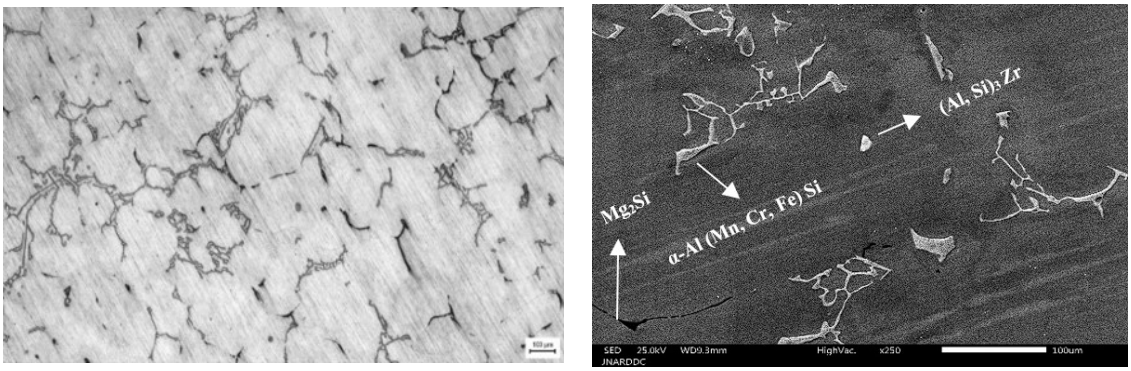

Figure 4. As-Cast microstructure. Left: Optical micrograph, Right: SEM image.

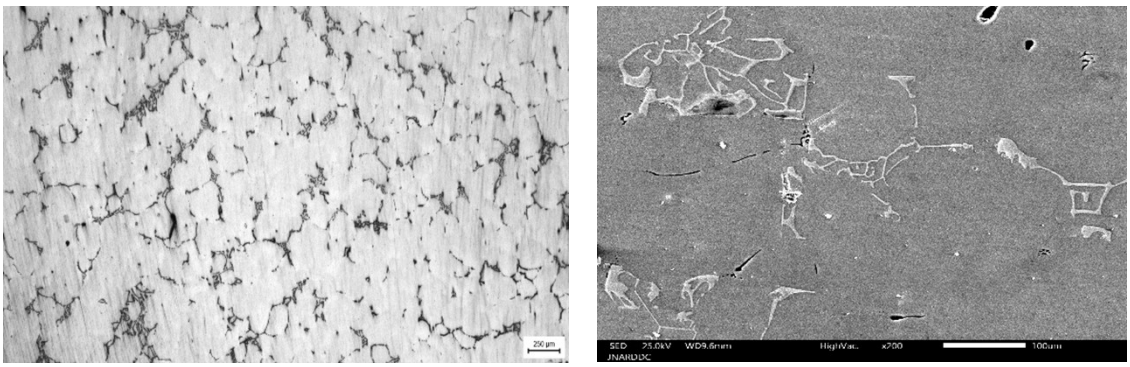

Figure 5. Homogenised sample. Left: Optical micrograph, Right: SEM image.

The tensile samples extruded at a ram speed of 1 mm/s exhibited high strength in both as extruded and T6 conditions. In the as-extruded state, the samples showed an average yield strength (YS) of 94 MPa, ultimate tensile strength (UTS) of 150 MPa, and elongation of 24 % (Figures 7 and 9). After T6 heat treatment, the samples demonstrated a significant increase in strength, with an

average YS of 301 MPa, UTS of 343 MPa, and an elongation of 18 %. in as extruded condition (Figures 8 and 9). The highest strength in the T6 condition was observed at a ram speed of 1 mm/s, YS of 314 MPa, UTS of 354 MPa and elongation of 16 %, which is attributed to the greater number of dislocations introduced into the material as a result of higher deformation during extrusion at this speed.

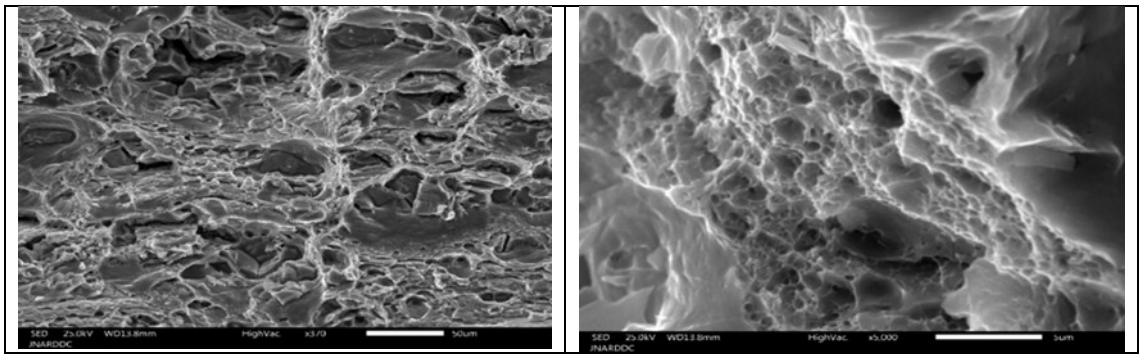

Figure 6. SEM image. Left: Large dimples due to α-Al(Fe, Mn, Cr) Si intermetallics. Right image: Small dimples due to (Al, Si)3Zr dispersoids.

Fractography studies on the tensile samples were conducted, and the corresponding SEM images are presented. The microstructure reveals dimples of varying sizes, with larger dimples observed near Mn-rich dispersoids and finer dimples located adjacent to Zr-rich dispersoids. The excess addition of zirconium (Zr) led to the formation of a greater number of Al_3Zr dispersoids, which effectively pin grain boundaries and inhibit recrystallization [11]. This suppression of recrystallization promotes the formation of a finer grain structure, ultimately enhancing the strength of the material. Dimples approximately 5–10 µm in diameter are observed in the fracture samples which are shown in Figure 6. Smaller dimples are also present between the larger ones, some of which contain intermetallic constituent particles at their centers.

Despite the T6 heat treatment, the material exhibited a notable ductility of 16 % at high ram speed of 1 mm/s, which is attributed to the presence of both large and fine dimples in the fracture surface in Figure 9. These dimples facilitated plastic deformation, thereby contributing to the overall elongation of the material. Samples extruded at higher speeds exhibited a greater number of fine dimples, attributed to the increased formation of dispersoids resulting from excess alloying additions. These dispersoids contributed to the formation of sub-micron-sized dimples, which in turn enhanced the material's strength.

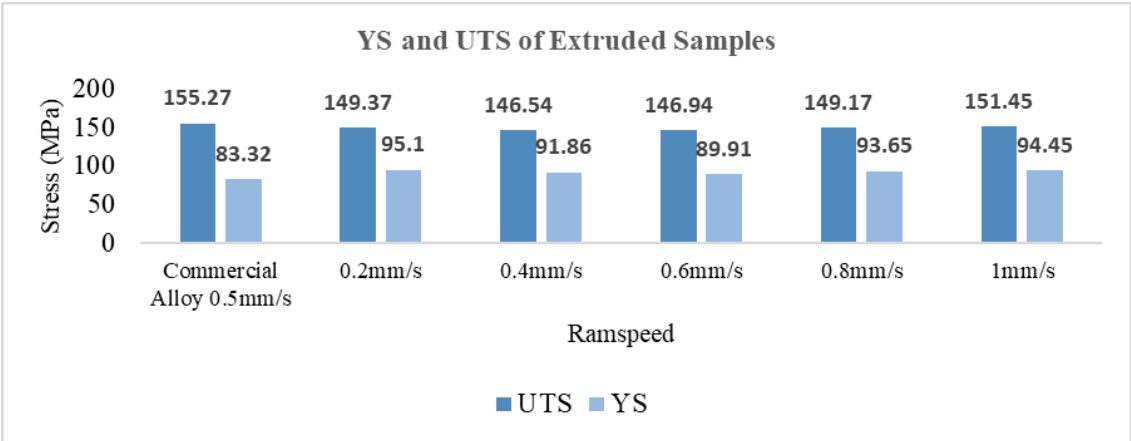

Figure 7. Yield strength (YS) and ultimate tensile strength (UTS) of as-extruded samples of commercial and developed alloy.

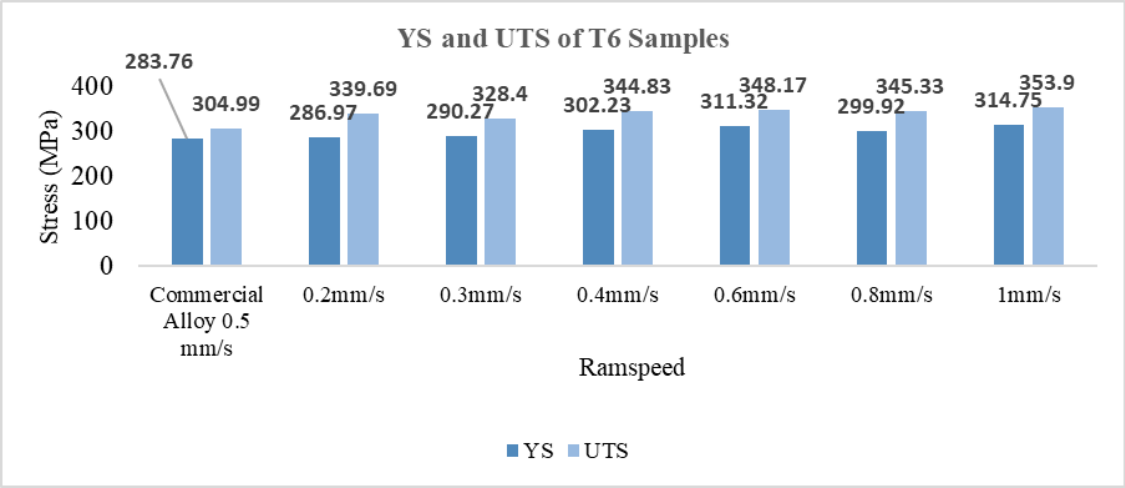

Figure 8. Yield strength and ultimate tensile strength of T6 samples of commercial and developed alloy.

The formation of the β-phase, typically a needle-shaped phase known to promote crack initiation and propagation, was significantly suppressed by the addition of zirconium (Zr). As a result, its presence was minimal. The high strength achieved in the developed alloy is attributed to the combined effects of grain boundary stabilization by Al_3Zr precipitates and α-Al (Fe, Mn, Cr) Si dispersoids, which retard grain growth at elevated temperatures. Additionally, age-hardening through Mg_2Si precipitation further contributes to both the strength and elongation of the alloy.

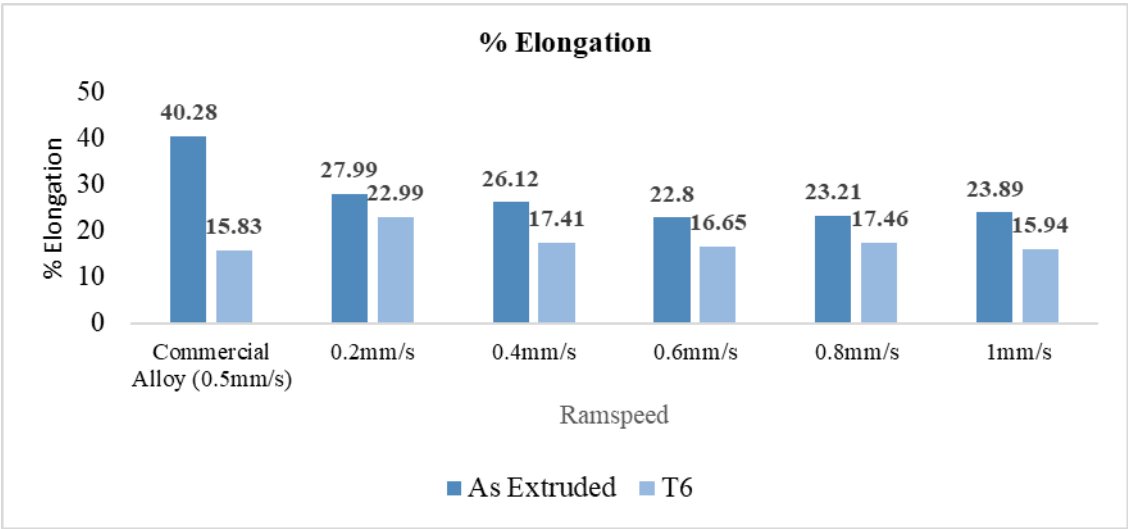

Figure 9. % Elongation for T6 and As-extruded samples for commercial and developed alloy.

4. Conclusions

In this study, more than 0.4 wt.% of zirconium (Zr) was added to an AA6082-based alloy, along with slight modifications to the major alloying elements such as magnesium (Mg), silicon (Si), and manganese (Mn). The thermodynamic simulations were performed using Fact Sage software and validated through the casting of billets measuring 150 mm in diameter and 400 mm in length, using a laboratory-scale casting facility without controlled cooling conditions. The conclusions drawn from the study are presented below.

The addition of excess zirconium resulted in the formation of DO23-type $(Al, Si)_3Zr$ precipitates, which are incoherent with the α-Al matrix. These dispersoids contributed to grain boundary pinning through the Zener drag effect, thereby enhancing the strength of the alloy. The excess addition of silicon (Si) and manganese (Mn) further enhanced the strength of the developed alloy through the formation of Mn-rich dispersoids and Mg_2Si precipitates via age hardening. These combined effects significantly contributed to both the strength and elongation of the alloy.

Extrusion of the developed alloy facilitated the breakdown of primary intermetallics formed during casting. Furthermore, Zr precipitates effectively suppressed high-temperature grain growth, leading to microstructural refinement and improved mechanical strength. Thermodynamic simulations were validated through experimental casting of the alloy, where the addition of zirconium resulted in a tensile strength improvement of approximately 50 MPa. It is anticipated that utilizing a proper direct chill (DC) casting facility will lead to further strength enhancements, which will be explored in future work.

5. References

1. Yi-Cheng Gao et al., Research progress, application and development of high performance 6000 series aluminium alloys for new energy vehicles, *Journal of Materials Research and Technology,* Volume 32, September–October 2024, 1868-1900. https://doi.org/10.1016/j.jmrt.2024.08.018
2. The Main 6xxx Aluminium Alloys in Aircraft Industry, https://www.aircraftaluminium.com/a/the-main-6xxx-aluminum-alloys-in-aircraft-industry.html (Accessed on 14 June 2024).
3. Jan Šmalc et al., The impact of small Zr addition to Al–Ni cast alloy for elevated temperature applications, *Journal of Materials Research and Technology, Volume 32,* September–October 2024, 1928-1936. https://doi.org/10.1016/j.jmrt.2024.08.029
4. Feng Wang et al., The grain refinement mechanism of cast aluminium by zirconium, *Acta Materialia,* Volume 61, Issue 15, September 2013, 5636-5645. https://doi.org/10.1016/j.actamat.2013.05.044
5. Yucel Birol, Effect of Cr and Zr on the Grain Structure of Extruded EN AW 6082 Alloy. *Journal of Metals and Materials International*, 2014, Volume 20, 727–732.
6. Florian Schmid et al., Synergistic alloy design concept for new high-strength Al–Mg–Si thick plate alloys, *Materialia*, Volume 15, March 2021, 100997.
7. Jovid Rakhmonov et al., Effects of Al (MnFe)Si dispersoids with different sizes and number densities on microstructure and ambient/elevated-temperature mechanical properties of extruded Al–Mg–Si AA6082 alloys with varying Mn content, *Journal of Alloys and Compounds,* Volume 861, 25 April 2021, 157937.
8. Franc Zupanič et al., Microstructure and Properties of a Novel Al-Mg-Si Alloy AA 6086, *Metals* 2021, 11(2), 368. https://doi.org/10.3390/met11020368.
9. Juan-Ricardo Castillo-Sánchez et al., Investigation of silicon sublattice substitution within (Al, Si)3 Zr intermetallic via DFT simulations, *2023 IOP Conf. Ser.: Mater. Sci. Eng.* 1281 012055. https://doi.org/10.1088/1757-899X/1281/1/012055
10. Xiaoming Qian, Nick Parson and X.-Grant Chen, Effects of Mn addition and related Mn-containing dispersoids on the hot deformation behaviour of 6082 aluminium alloys, *Journal of Materials Science and Engineering: A,* Volume 764, 9 September 2019, 138253. https://doi.org/10.1016/j.msea.2019.138253
11. L. Lityńska-Dobrzyńska et al., Structure and properties of Al-Mg-Si alloys with Zr and Sc additions produced by melt spinning and twin rolling casting techniques, *Kovove Mater.* 48, 2010, 9-15, https://doi.org/10.4149/km_2010_1_9.